# Effect of seawater diffusion on the dielectric properties of silicone elastomer

E. Taine, T. Andritsch, Senior Member, IEEE, and I. A. Saeedi, Member, IEEE

Abstract-This study investigates the diffusion kinetics of seawater into silicone dielectric elastomers and their detrimental effects on electromechanical performance in energy harvesting applications. Encapsulated dielectric elastomer samples were prepared and immersed in water to correlate DC resistivity changes with water content diffusing through the membrane. Results demonstrate that water ingress induces significant conduction losses, which are similar in both seawater and deionized water. When considering the use of these materials for ocean energy harvesting, conduction losses reduce the transducer efficiency. Therefore, the dielectric properties of water-saturated samples were analyzed under typical electro-mechanical harvesting schemes, highlighting severe limitations at low stretch amplitudes. Furthermore, water-saturated samples exhibited a 22% reduction in dielectric breakdown strength, substantially diminishing the achievable energy density of submerged generators such as wave energy converters.

Index Terms—Seawater diffusion, electrical resistivity, silicone, conversion efficiency, dielectric breakdown strength.

### I. INTRODUCTION

PARTICULAR interest has been shown to deploy dielectric elastomer (DE) transducers in marine environment as fully submerged flexible robots [1]–[3], wave energy converters [4]–[6] or underwater sensors [7]. Among the various materials used for DE applications, polydimethylsiloxane (PDMS) stands out as a promising candidate due to its its good resistance to chemical ageing, mechanical fatigue, and its low dielectric and mechanical losses [8]–[10].

In generator mode, DE transducers cyclically convert mechanical strain energy—induced by external forces such as ocean waves—into electrical energy through cyclic changes in capacitance. This process requires the elastomer to maintain high electrical insulation under strong electric fields, often exceeding tens of volts per micrometer. Further details on the harvesting principle and associated electronics can be found in the comprehensive review by Moretti et al. [11]. Despite PDMS's hydrophobic nature, it remains permeable to water vapor [12], [13], which poses a challenge for submerged applications. Water ingress can alter the dielectric properties of the elastomer, potentially degrading energy conversion efficiency and long-term reliability. While the effects of humidity on dielectric breakdown strength (DBS) have been

This paper was produced by the IEEE Publication Technology Group. They are in Piscataway,  $\ensuremath{\mathsf{NJ}}.$ 

Manuscript received April 19, 2021; revised August 16, 2021.

studied [14]–[16], the impact of full submersion—particularly in seawater—remains unexplored.

This study addresses that gap by introducing a novel encapsulated sample design that allows water diffusion into the dielectric layer while preventing direct contact between electrodes and water. This enables continuous monitoring of DC resistivity and DBS under submerged conditions. Although recent demonstrations of submerged PDMS-based generators [17] have shown the feasibility of underwater energy harvesting, the influence of water diffusion on systemlevel efficiency has not yet been quantitatively assessed. The manuscript is structured to first detail the sample preparation and experimental methodology, followed by an analysis of water diffusion kinetics and their correlation with electrical resistivity. The implications of water-induced conduction losses on the efficiency of the DE generator are then evaluated for representative harvesting schemes and operating conditions. Finally, the study quantifies the reduction in DBS due to seawater exposure and discusses its impact on the reliability of submerged DE systems.

## II. METHOD

The rapid water diffusion within a DE membrane of a few hundred micrometers thickness presents a significant challenge for precise measurements due to its brief timescale (typically within a few seconds). To address this issue, the DE layer was encapsulated within a thicker silicone coating. This approach serves multiple purposes: it prevents direct contact of the electrodes with water, enables watertight electrical connections, decelerates water uptake at the DE layer, thereby enabling consistent monitoring of mass and dielectric property changes over time. In this design, the DE layer thickness is negligible compared to that of the encapsulation layer. Consequently, the water concentration gradient across the DE layer can be approximated as negligible, which enables establishing a direct relationship between water content and electrical resistivity. Furthermore, the encapsulated design permits in situ monitoring of electrical properties while the sample remains submerged, thereby eliminating potential errors associated with handling or transferring the sample between the immersion tank and external measurement equipment.

## A. Sample preparation

The analysis was conducted on silicone film fabricated from liquid silicone rubber (LSR) with a shore hardness of 50 ShA. The film has a thickness at rest of  $d_0 = 105 \pm 3\mu m$ . In this film, samples are cut such as obtaining membrane of 290 mm length and 190 mm width. Then, a compliant electrode made of a commercially available conductive silicone was coated over the dielectric PDMS using an ultrasonic spraying nozzle actuated by a three-axis motor (Fig. 1(a)). The coating is cured 20 minutes at 110°C such as removing the solvent residuals and crosslinking the coated silicone. The electrode is smaller than the surface of the dielectric film such as preventing shortcircuit or electrical breakdown between the electrodes of opposite polarities and a clearance of 20 mm is respected between the electrode termination and the edge of the dielectric membrane. Thickness of the final electrode is measured at 30  $\mu$ m.

A first electrical connection is made between the electrode and a silicone insulated aluminium wire. The cable termination is stripped and glued to the electrode conductive LSR silicone such as allowing electrical measurements on the DE in its final arrangement. The sample is installed in a poly(methyl methacrylate) mould, and a ultra-violet (UV) curing silicone is injected to fill the cavity, ensuring that the electrode and its wire connection are completely encapsulated (Fig. 1(b) and Fig. 2(a)). This barrier will avoid direct contact of the electrode to water once the samples are immersed (thickness of the encapsulation layer is 8.5mm on both sides of the DE layer). Outer surface of the mould is exposed to UV radiation and its transparency in the UV wavelength allows the crosslinking reaction to occur and the silicone to harden (Fig. 1(c)). The mold is re-opened, the sample flipped upside down, and the carrier film is peeled from the dielectric elastomer. Subsequently, the second electrode is coated (Fig. 1(d)), cured, connected, and encapsulated following the same procedure (Fig. 1(e)). A slight offset in the coating position of the second electrode is realized such as avoiding superposition of the two electrode edges and more importantly of two electrical connections (these inhomogeneities would otherwise be prone to premature electrical failures because of electric field enhancements at these locations). Finally, the mould is completely removed and a thin spray of conductive silicone is coated on the outer surface of the sample (using the same process used for electrode deposition) which serves as a guard electrode during DC resistivity measurement (Fig. 1(f)). The final assembly is post-cured 15 hours at 110°C resulting in a silicone encapsulated, watertight DE sample (Fig. 2(b)).

# B. Test environment

Once samples are completed, the elastomer remains susceptible to moisture uptake, which can be influenced by fluctuations in the laboratory's relative humidity. Therefore,

the initial water content in the sample remains unknown and in that purpose, samples have been stored in vacuum chamber for a duration of 30 days such as obtaining a fully dried reference case.

After this conditioning operation, the samples are fully

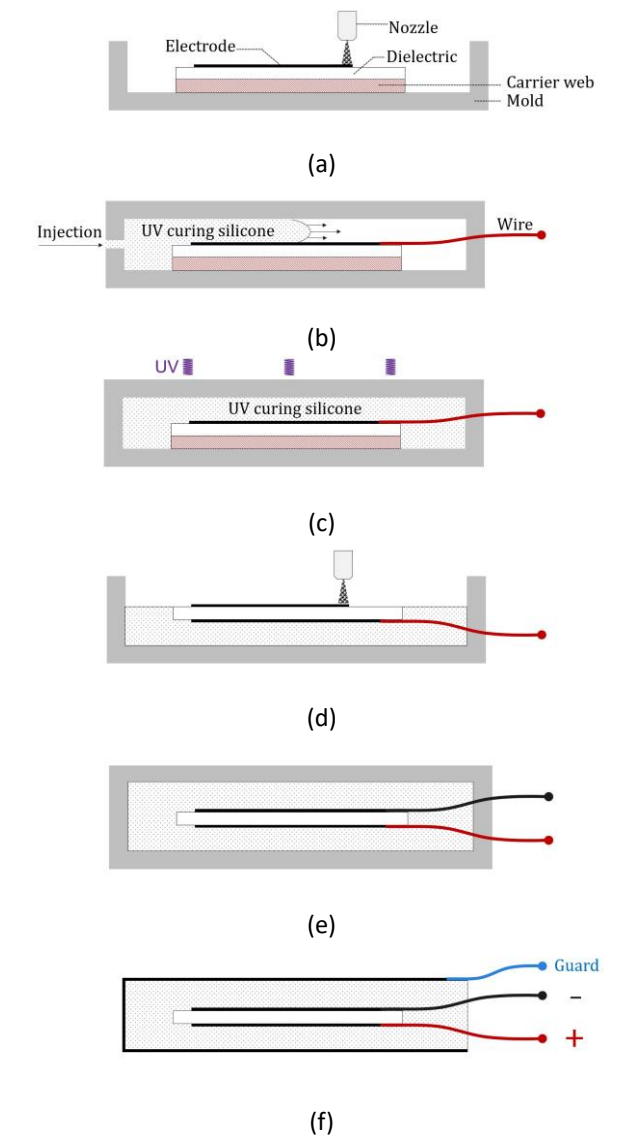


Fig. 1. Schematic of the sample preparation (dimensions not at scale). (a) Electrode coating. (b) Overmolding operation. (c) UV curing of the encapsulation. (d) Opposite electrode coating. (e) Final overmolding injection and curing. (f) Final sample after the guard electrode coating.

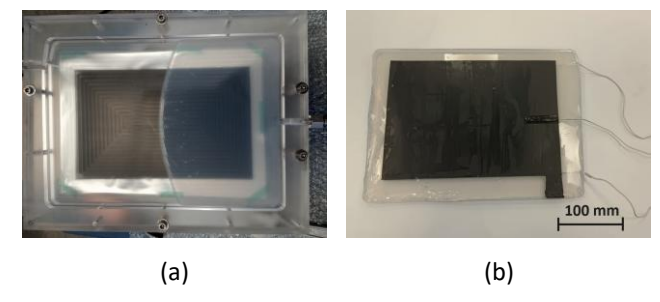


Fig. 2. Sample preparation. (a) Overmolding operation. (b) Final sample with its guard electrode.

submerged in a tank filled with substitute ocean water prepared following the requirement of ASTM-D1141. Mass of the samples are measured on a regular basis using a precision scale. Before the mass measurement, samples are wiped with a paper tissue to remove excess of water that remains on the surface. The same measurement procedure was replicated on samples immersed in deionized water. The deionized water used in this process is characterized by an electrical conductivity lower than 1  $\mu$ S.cm<sup>-1</sup> and complies with the DIN 43530 standard for high-quality water used in industrial applications. To put this value in perspective, the conductivity of the deionized water used is approximately five orders of magnitude lower than that of typical ocean water [18].

After reaching full saturation, the samples of the two tested media were returned to the vacuum chamber. Their masses were then measured at regular intervals to assess the kinetics of the desorption process.

# C. DC resistivity measurement

The DC resistivity measurement was conducted using an insulation tester (Megger S1-1068). The experimental setup involved connecting two electrodes to the positive and negative outputs of the tester under an applied DC voltage of 1000V (corresponding to an electric field of 9.5 V. $\mu$ m<sup>-1</sup> across the DE), while the sample's outer surface was linked to the guard terminal of the measuring instrument. Measurements were taken at a sampling frequency of 1 Hz. Prior to immersion, the sample underwent a crucial preparation step. It was exposed to an electric field within a vacuum chamber (1000V across opposite electrodes), in order to eliminate polarisation currents and to ensure that the subsequent measurements primarily captured the conduction current. This preparatory phase typically lasted around 6 hours, during which a steadystate current was rapidly established, as illustrated in Fig. 3 for two distinct samples. Following this preparation, the sample was carefully immersed in the test medium without interrupting the applied electric field. Throughout the immersion process, resistance values continued to be recorded at the same 1 Hz frequency. This methodology allowed for a seamless transition between the pre-immersion and immersion stages, maintaining the integrity of the electrical conditions throughout the experiment. The guard electrode has proven to be an essential component in ensuring stable current measurements during the transition phase. Its primary function is to maintain a constant and controlled potential at the sample's outer surface and prevent polarisation of the encapsulation layer to occur at the immersion stage.

# III. RESULTS AND DISCUSSION

# A. Water diffusion

After immersion in the tank, the mass of the samples  $m_t$  was regularly measured and compared to their initial value before

immersion  $m_0$ . The water uptake (1) stabilized at  $0.16 \pm 0.01$  wt% after approximately 100 hours in both tested media (seawater and deionized water). Although the samples comprise multiple silicone components, these curves are considered representative of the diffusion kinetics into the

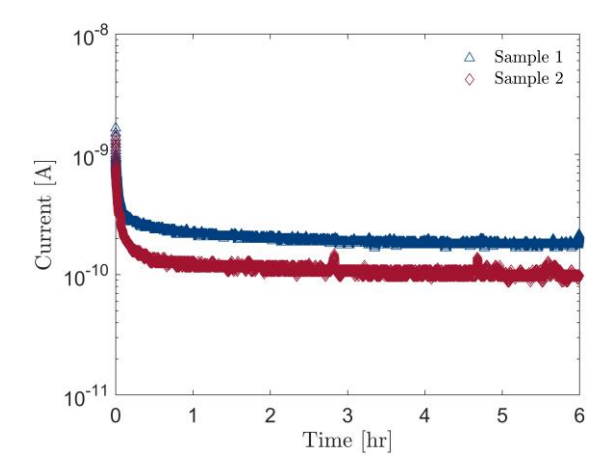


Fig. 3. Polarisation currents measured within the vacuum chamber (under a DC voltage of 1000 V).

encapsulation silicone, as this elastomer constitutes more than 99% of the sample volume. These data will be used to estimate the time required for water to reach the central DE layer. However, in the subsequent analysis, the water content in the DE material also remains of particular importance. Consequently, additional samples only constituted of this elastomer were prepared to measure and compare water diffusion into this distinct material (Fig. 4).

$$\frac{\Delta m}{m_0} = \frac{m_t - m_0}{m_0} \tag{1}$$

The coefficient of diffusion D is determined from the experimental results using the Fick's second law (2) with c the water concentration at position x across thickness of the sample.

$$\frac{\partial c}{\partial t} = D \frac{\partial^2 c}{\partial x^2} \tag{2}$$

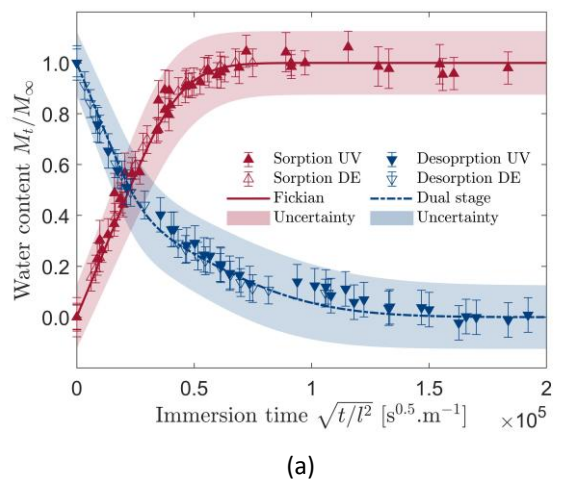
Given the geometry of the sample, the case is simplified to a diffusion problem in an infinite plate (i.e. diffusion in the edges of the samples are considered negligible relatively to the water diffusion across the larger surfaces). After defining the central position of the DE as x=0 and the outer surfaces of the sample as  $x=\pm l$ , the solution for equation (2) can be expressed as (3) with  $M_t$  the mass of the diffusing substance at a diffusion time t, and  $M_{\infty}$  the corresponding quantity after infinite time (i.e at saturation) [19]. The diffusion coefficient is obtained by fitting this equation to the experimental mass measurements as represented in Fig. 4(a) for the seawater and in Fig. 4(b) for the deionized water environment.

$$\frac{M_t}{M_{\infty}} = \left[1 - \sum_{n=0}^{\infty} \frac{8}{(2n+1)^2 \pi^2} e^{-D(2n+1)^2 \pi^2 t/4l^2}\right]$$
(3)

The diffusion kinetic appears very similar between the two tested media and the two elastomers. Therefore, in the following analysis a unique value of  $D=3.9\times10^{-10}~\text{m}^2.\text{s}^{-1}$  was considered for the sorption process. Taking into account the inherent uncertainties in the mass measurement protocol (water residual on the surface of the sample) and the

evolution of water content at the position of the dielectric elastomer layer (x=0) reveals three distinct phases, as illustrated in Fig. 5(a). When focusing on the sorption process, the phases can be interpreted as follow:

- Phase (I): A first phase, lasting approximately 2 hours, where the water front has not yet reached the DE layer, maintaining its initial dry state.
- Phase (II): A transitional phase where the water



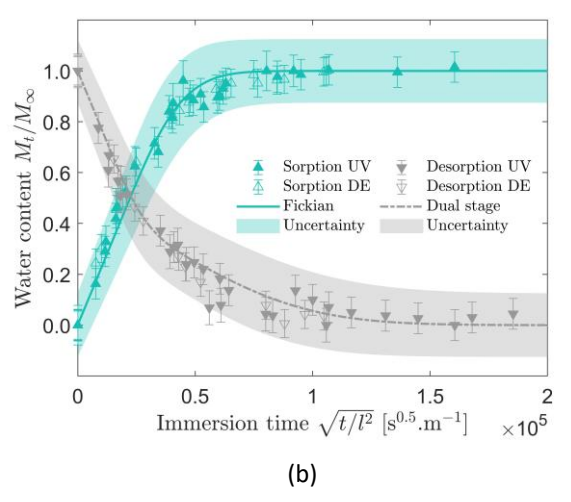


Fig. 4. Water diffusion in silicone elastomers under experimental conditions and modeled diffusion in two distinct media: (a) Seawater and (b) Deionized water. UV represents the encapsulation silicone, while DE refers to the dielectric elastomer silicone.

limitations of the accuracy of the scale, a relative error of  $\pm 20\%$  has been applied to the calculated diffusion coefficient. This margin of error combines with the error in the value of the water content at saturation and is visually represented by the light-coloured surfaces surrounding the primary diffusion curves in Fig 4.

During the desorption process, the experimental data does not obey the same Fickian diffusion process observed during the water sorption. More complex phenomena are at play, and different models have been evaluated to best represent the desorption kinetic. From analysing the data, the following observations are made: in the initial desorption stage, the behaviour looks reversible of the sorption process (from  $\frac{M_t}{M_{CO}}=1_{10}$ 

 $\frac{M_t}{M_\infty}=0.5$  ), then in a second stage the desorption slows down and it takes much longer to desorb the residual water amount (from  $\frac{M_t}{M_\infty}=0.5$  to  $\frac{M_t}{M_\infty}=0$ ). For such behaviour, Placette et al. have proposed combining two Fickian terms [20], and the resulting dual stage model represents the experimental data much better than a single Fickian process. Description of the model and the fitting parameters used are further detailed in Appendix.

By applying the solution presented in (3) and (13) to the specific geometry of our sample, we can derive a comprehensive profile of water concentration across the sample's thickness at various sorption times. The temporal

- concentration gradually increases as water molecules progressively diffuse through the dielectric elastomer.
- Phase (III): A final phase representing the equilibrium state where the sample reaches full saturation. In this stage, the water content stabilizes at approximately 0.16 wt% (it was verified that the water content at saturation were equal in both the encapsulation silicone and the DE silicone).

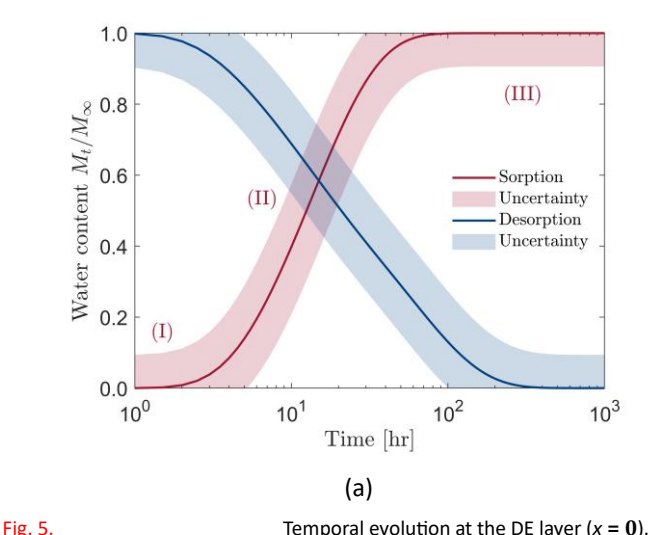
The observed water content evolution at the DE layer provides input for the subsequent analysis where the water concentration will be related to the change in electrical properties. The next section explores how DC resistivity changes as water diffuses through the central DE layer.

## B. DC resistivity

After the initial polarisation realized under vacuum, the sample is immersed in seawater and the DC resistance evolves according the the red markers represented in Fig. 5(b) (the light red surface represents the accuracy of the measuring device). The three distinct phases identified in time evolving water content at the DE layer are also clearly visible in the resistance curve indicating a correlation between the two measurements. To evaluate the possible reversibility of the process, the same sample is put back in the vacuum chamber once fully saturated and the same measurement is repeated during the desorption

process as represented by the blue markers in Fig. 5(b). Interestingly, the change of resistance measured during the desorption process is not entirely symmetrical to the behaviour observed during the sorption stage. Particularly, the timescale of the change of resistance is longer for the desorption process similarly to what was previously described for the mass change.

After combining the results presented in Fig. 5(a) and Fig. 5(b), the relation between water content at the DE layer and DC resistivity can be determined (Fig. 6). The electrical resistivity  $\rho_e$  is obtained from the value of the electrical capacitance C of the sample as given in (4). And the accuracy of the analysis is again represented with the coloured surface and combines the different sources of error (i.e. the error on the



measurements in seawater.

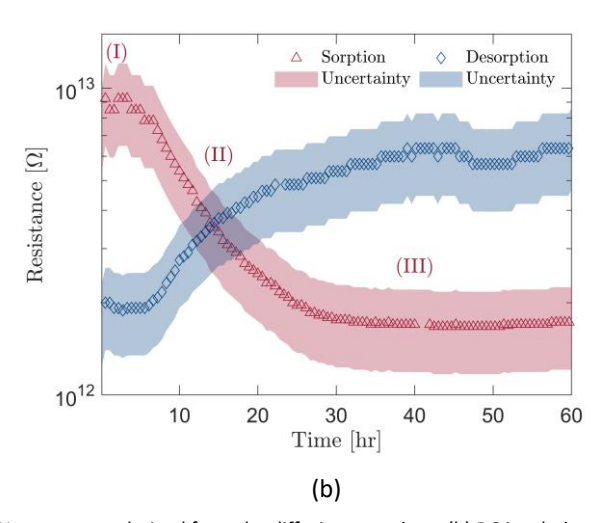
diffusion coefficient ( $\pm$  20%), the error on the water content at saturation ( $\pm$  0.01 wt%) and the error on the position of the DE layer inside the encapsulation material ( $\pm$  1 mm).

$$\rho_e = \frac{RC}{\varepsilon} \tag{4}$$

The precise role of ionic species in the observed changes in DC resistivity remains uncertain. To better assess their relative importance, we conducted a comparative study using samples immersed in deionized water. These findings reveal striking similarities between the two media. The overall trend of electrical resistivity versus water concentration is remarkably consistent across both saline and deionized water environments (Fig. 6(b)). Furthermore, the electrical resistivity values of fully saturated elastomers are comparable, measuring approximately  $6\pm3\times10^{14}\,\Omega$ m in both cases despite the large difference in electrical resistivity of the two media. These observations suggest several implications. Common ionic species such as sodium cations or chloride anions likely do not significantly contribute to the variations in DC resistivity.

Instead, the changes in resistivity may be attributed to other ionic species present in similar concentrations in both media such as protons generated by the dissociation of water [21]. In practical DEG applications, the applied electric field varies with time, potentially giving rise to dielectric relaxation phenomena—such as dipolar relaxation of diffused water molecules. These frequency-dependent effects are not directly captured by our DC resistivity measurements but merit further investigation using techniques like dielectric spectroscopy in future studies.

The next section aims to assess the consequences of the observed decrease in resistivity on a representative dielectric elastomer generator operated underwater and to analyse the associated loss of conversion efficiency.



Temporal evolution at the DE layer (x = 0). (a) Water content derived from the diffusion equations. (b) DC insulation resistance

C. Implications of losses at a system level

Dielectric elastomer generators (DEGs) are particularly well-suited for harvesting energy from low-amplitude, largemotion oscillations, making wave energy conversion a promising application aligned with these operational characteristics. Silicone-based dielectric materials have been implemented in fully submerged generators like the S3 $^*$  wave energy converter [5]. When operated underwater, dielectric elastomers rapidly become saturated with water, significantly reducing the insulation resistance of the dielectric layer under applied electric fields. The flow of conduction current through the water-saturated dielectric material leads to energy dissipation in the form of heat, known as Joule heating or resistive heating. The power of these Joule losses P(t) can be calculated using (5) with i(t) the conduction current and V(t) the voltage across the dielectric.

$$P(t) = V(t)i(t) \tag{5}$$

Assuming that the conduction current obeys to an Ohmic behaviour (resistivity independent of the applied electric field), equation (5) can be rearranged to (6) with A(t) the time varying

surface of the overlapping electrodes and d(t) the time varying thickness of the dielectric. Assuming volume conservation of the dielectric  $A(t)d(t) = \Omega$ , and a uniform electric field across the electrodes E(t) = V(t)/d(t), the heat power attributed to conduction losses is finally given by (7).

$$P(t) = \frac{V(t)^2}{R(t)} = \frac{V(t)^2 A(t)}{\rho_e d(t)}$$
 (6)

$$P(t) = \frac{E(t)^2 \Omega}{\rho_e} \tag{7}$$

The energy dissipated into conduction losses  $W_c$  over an entire harvesting cycle of period T is obtained after integrating (7), yielding in (8).

$$W_c = \int_t^{t+T} P(t) dt = \frac{\Omega}{\rho_e} \int_t^{t+T} E(t)^2 dt$$
 (8)

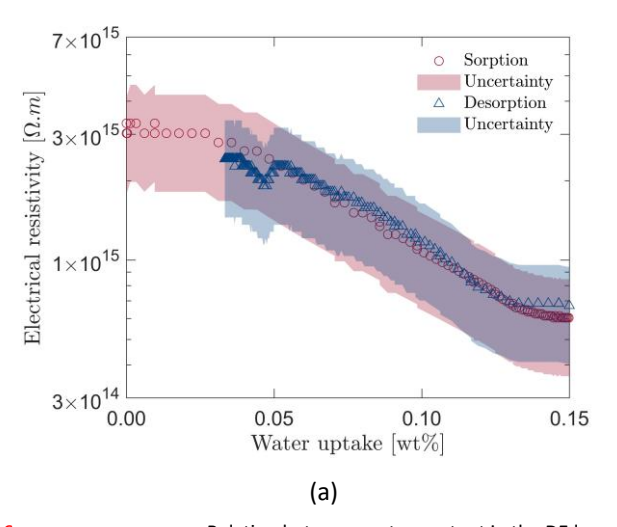


Fig. 6. Comparison of seawater and deionized water during sorption.

To determine to what extent these losses are detrimental in the energy conversion efficiency of a DEG, this number has to be compared to the net energy converted  $W_e$  (assuming no conduction losses). Let us define an electrical loss ratio  $\phi_e$ representing the ratio of conduction losses to the net energy converted (9).

$$\phi_e = \frac{W_c}{W_e} \tag{9}$$

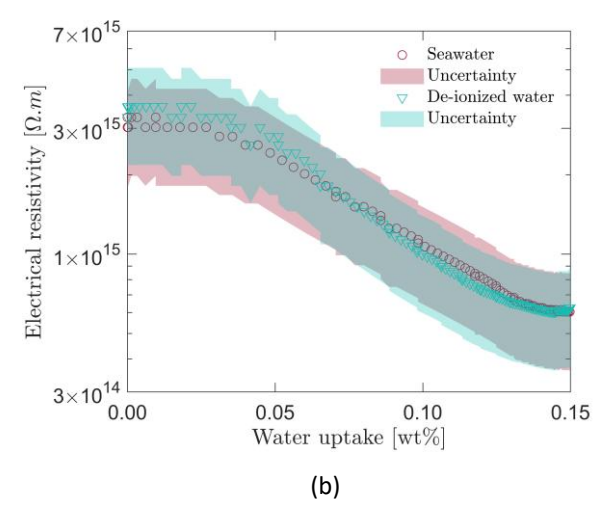
The analysis was conducted for two typical harvesting schemes [11]: the most energetic constant electric field cycle (CE) and the simpler-to-implement but less energetic constantcharge constant-voltage cycle (CCCV). For a comprehensive overview of these conversion cycles and their respective energy conversion equations, see [11]. After substituting  $W_e$  using the energy density equations of each

cycle, the electric loss ratios given in (10) and (11) are obtained for each harvesting scheme.

$$\phi_{e,CE} = \frac{W_c}{W_{e,CE}} = \frac{\int\limits_t^{t+T} E(t)^2 dt}{\rho_e \varepsilon E_{max}^2 ln \sqrt{\hat{\beta}}}$$
(10)

$$\phi_{e,CCCV} = \frac{W_c}{W_{e,CCCV}} = \frac{\int\limits_t^{t+T} E(t)^2 dt}{\rho_e \varepsilon E_{max}^2 \left(1 - \frac{1}{\sqrt{\hat{\beta}}}\right)^2}$$
(11)

Assume a typical DEG that makes up part of the tubular S3° wave energy converter [5]. For such a system, the principal stretch is a result of a diameter change (whereas the length of the tube remains unchanged) meaning that the capacitance swing equals  $\hat{\beta} = (\lambda_{max}/\lambda_{min})^2$ . For a typical loading condition given in Table I, where the waves cause a sinusoidal expansion



Relation between water content in the DE layer and electrical resistivity. (a) Comparison of sorption and desorption in seawater. (b) of the diameter (Fig. 7(a)), the electric field along a cycle varies according to Fig. 7(b). Calculating the integral of E(t) using a numerical integration and inserting the result

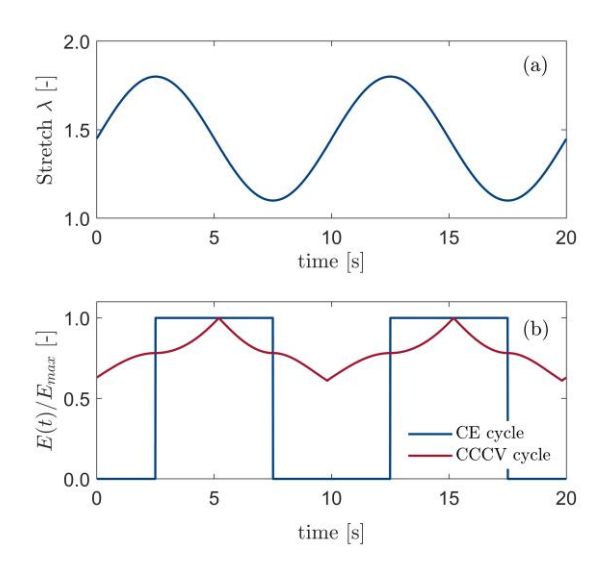


Fig. 7. Calculation of conduction losses along a CE cycle and a CCCV cycle. (a) Stretch variation. (b) Electric field profile.

obtained into (8) gives the energy density dissipated into heat. For the specific conditions of Table I,  $W_c$  represents 83 J.m<sup>-3</sup> for a CCCV cycle representing respectively 2.3% and 9.4% of the theoretical net energy output.

TABLE I

PARAMETERS USED TO DERIVE THE CONDUCTION LOSSES.

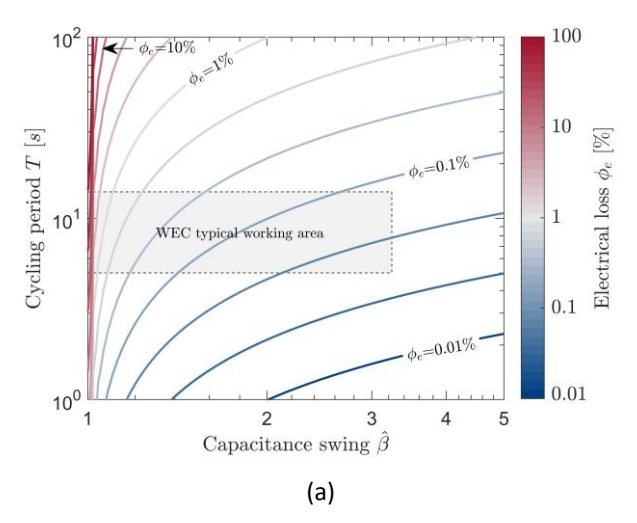
Parameter	Symbol	Value	Unit
Cycle period	T	10	S
Minimal stretch	$\lambda_{min}$	1.1	-
Maximal stretch	$\lambda_{max}$	1.8	-
Capacitance swing	$eta$ ^	2.7	-
Electrical resistivity	ho e	6×10 <sup>14</sup>	$\Omega$ .m
Permittivity	ε	$2.7 \times 8.854 \times 10^{-12}$	F.m-

The electrical loss ratio in a DEG is influenced by two key parameters: the capacitance swing and the cycling period. A longer cycle allows more time for current to flow through the dielectric, resulting in higher cumulative losses. These dependencies are illustrated in Fig. 8. In the context of wave energy, where waves typically cause cyclic stretching with periods between 5 and 14 seconds, the loss ratio is generally acceptable for larger capacitance swings. However, this observation does not hold for very low capacitance swings. For small stretch amplitudes, the minimal energy output barely compensates for the electrical conduction losses. This effect is particularly pronounced in the CCCV cycle, as illustrated in Fig. 8(b). In this case, the electrical loss ratio  $\phi_e$  can exceed 100% within the typical operating range of a S3° system, indicating that conduction losses surpass the maximum recoverable electrostatic energy. These findings have significant implications for the design and operation of DEGs, specifically,

for capacitance swings  $\hat{\beta} \leq 1.05$ , where there is no energetic benefit in charging the DEG.

# D. Dielectric breakdown strength

Once fully saturated, the samples described in Section II-A are left submerged in a seawater tank for a minimum duration of 500 hours (more than 10 times the saturation time). Following the submersion period, a voltage ramp-up of 500 V·s<sup>-1</sup> is applied across the opposite electrodes using the dielectric breakdown tester described in [22]. The dielectric breakdown strength was measured on 9 individual submerged samples. For comparison, measurements were also taken on identical samples stored in a controlled atmosphere at 23 °C and 50% relative humidity. The results of these measurements are presented in Fig 9 and fitted with a 2-parameters Weibull distribution (12). A clear degradation in the breakdown strength is observed for the submerged samples. This degradation manifests as a noticeable reduction in both the scale and shape parameters of the Weibull distribution (Table



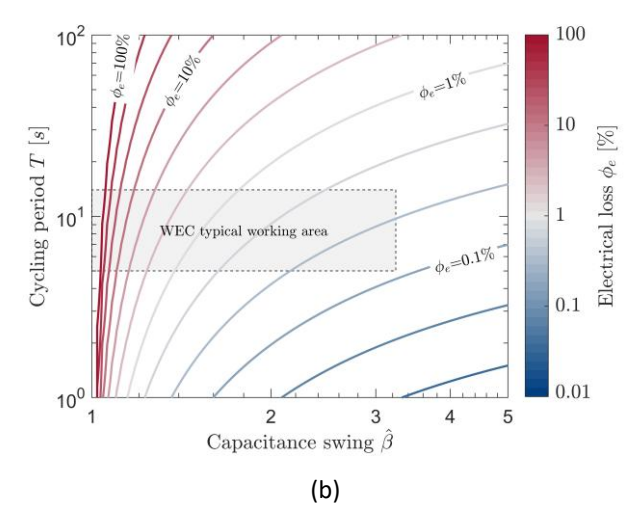


Fig. 8. Electrical loss ratio  $\Phi_e$  within working range of a typical wave energy converter. (a) CE cycle. (b) CCCV cycle.

II). The 22% reduction in the scale parameter indicates a decrease in the overall dielectric strength of the material when exposed to seawater. The change in the shape parameter

TABLE II PARAMETERS OF THE

WEIBL	JLL DISTRIBUTIONS.			
Parameter		Symbol ValuUnit		
				e
	Scale Dry		η	94 V.μm
			β	-1
	Shape	5.5	_η	$73 \mu m$
Seawater	Scale		B	-1
	Shape	3.7	•	

reveals an increase in the variability of the breakdown strength across the tested samples. It is worth noting that the relatively low beta value measured in this study, compared to previous studies on the same material [23], is primarily attributed to the large surface area of the electrodes. Although the mechanisms at play are not fully understood, recent studies have shed light on the potential mechanisms behind the observed behaviour of wet silicone samples. Zhang et al. conducted experiments that revealed an accumulation of space charge in wet PDMS, leading to local electric field distortion across the dielectric's thickness [24]. Notably, the reported field distortion culminates between 20% and 30% for post-cured PDMS, which closely aligns with the magnitude of DBS reduction observed in our experiment. This comparison provides a first insight on the role of space charge accumulation in the decreased dielectric strength of saturated PDMS samples.

$$U = 1 - e^{-\left(\frac{E}{\eta}\right)^{\beta}} \tag{12}$$

### IV. CONCLUSION

Our investigation has yielded several findings regarding the relationship between water content and the dielectric properties of the silicone material. A clear and direct relationship has been established between the water content and the DC resistivity of the elastomer. The reduction in resistivity is driven by a diffusion process, and we have demonstrated that this variation is reversible. Importantly, identical results were obtained using deionized water, allowing

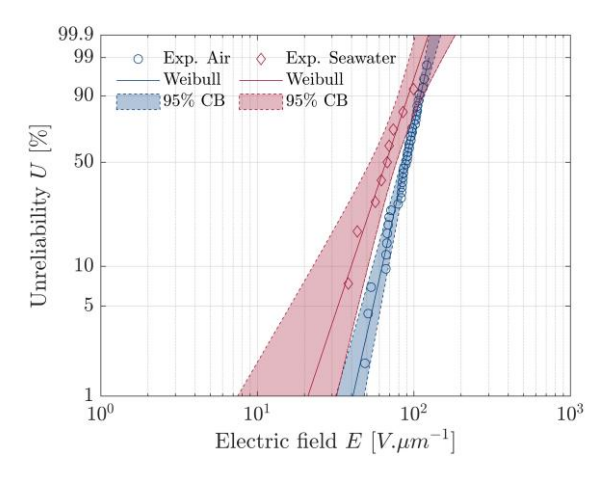


Fig. 9. Experimental DBS fitted with a Weibull distribution and its 95% confidence bound interval (CB).

us to rule out the role of chloride and sodium ions in the electrical degradation process. We further analyzed the effect of this resistivity reduction on DEG efficiency across various energy harvesting schemes and operating ranges. Our findings indicate that, except at very low capacitance swings, the impact on overall system efficiency is minimal.

Upon full saturation, we observed a marked reduction in the dielectric breakdown strength. This reduction was characterized by a combined decrease in both the shape and scale parameters of the Weibull distribution, indicating a weakening of the electrical reliability once exposed to an electric field for the submerged condition. The reduction measured in the DBS of water saturated samples is of similar magnitude as the electric field enhancement resulting from space charge accumulation reported in literature on a similar LSR silicone.

These findings highlight the significant impact of prolonged seawater exposure on the dielectric properties of the material, emphasizing the importance of considering environmental factors in the design and application of insulation systems in marine or high-humidity environments. Real-world marine environments involve more complex factors such as variations in temperature, hydrostatic pressure, and cyclic mechanical stretch. These parameters could influence both water diffusion kinetics and the microstructural state of the elastomer, potentially affecting dielectric properties and durability in ways not captured here. This highlights the need for further investigation under such realistic service conditions.

## **ACKNOWLEDGMENTS**

This was supported by SBM Offshore in the framework of the S3<sup>®</sup> wave energy converter project.

# APPENDIX DUAL STAGE DESORPTION

A dual stage desorption model was proposed by Placette *et al.* [20]. The model combines two Fickian terms (13) with  $D_1$  and  $D_2$  the diffusion coefficients of each stage and  $c_{sat,1}$  and

TABLE III PARAMETERS OF THE

DUAL STAGE DESORPTION.			
Parameter	Symbol	Value	Unit
Diffusion coefficient stage 1	$D_1$	6.5×10 <sub>-10</sub>	m2.s-1
Diffusion coefficient stage 2	$D_2$	1.2×10-10	m2.s-1
Transition stage	$\frac{0,1}{M_{\infty}}_{M}$	0.5	-

 $c_{\mathit{sat},2}$  the concentration at saturation of each stage. The model parameters fitted to our experimental desorption data are given in Table III.

 $c(x,t)=c_1(x,t,D_1,c_{sat,1})+c_2(x,t,D_2,c_{sat,2})$  (13) The equation for  $\frac{M_t}{M_\infty}$  is then given by (14)

$$\frac{M_t}{M_{\infty}} = \frac{M_{0,1}}{M_{\infty}} \left[ \sum_{n=0}^{\infty} \frac{8}{(2n+1)^2 \pi^2} e^{-D_1(2n+1)^2 \pi^2 t/4l^2} \right] + \frac{M_{0,2}}{M_{\infty}} \left[ \sum_{n=0}^{\infty} \frac{8}{(2n+1)^2 \pi^2} e^{-D_2(2n+1)^2 \pi^2 t/4l^2} \right]$$
(14)

with

$$\frac{M_{0,2}}{M_{\infty}} = 1 - \frac{M_{0,1}}{M_{\infty}} \tag{15}$$

## **REFERENCES**

- J. Shintake, H. Shea, and D. Floreano, "Biomimetic underwater robots based on dielectric elastomer actuators," in 2016 IEEE/RSJ International Conference on Intelligent Robots and Systems (IROS), Conference Proceedings, pp. 4957–4962.
- [2] H. Godaba, J. Li, Y. Wang, and J. Zhu, "A soft jellyfish robot driven by a dielectric elastomer actuator," *IEEE Robotics and Automation Letters*, vol. 1, no. 2, pp. 624–631, 2016.
- [3] F. Berlinger, M. Duduta, H. Gloria, D. Clarke, R. Nagpal, and R. Wood, "A modular dielectric elastomer actuator to drive miniature autonomous underwater vehicles," in 2018 IEEE International Conference on Robotics and Automation (ICRA), Conference Proceedings, pp. 3429–3435.
- [4] G. Moretti, G. Rosati, L. Daniele, D. Forehand, D. Ingram, R. Vertechy, and M. Fontana, "Modelling and testing of a wave energy converter based on dielectric elastomer generators," *Proceedings of The Royal Society A*, vol. 475, 2019.
- [5] P. Jean, A. Wattez, G. Ardoise, C. Melis, R. Van Kessel, A. Fourmon, E. Barrabino, J. Heemskerk, and J. P. Queau, "Standing wave tube electro active polymer wave energy converter," in SPIE Smart Structures and Materials +Nondestructive Evaluation and Health Monitoring, vol. 8340, Conference Proceedings, pp. 75–95.
- [6] S. G. Bauer and C. Keplinger, "Dielectric-elastomer actuators deliver clean energy," SPIE Newsroom, 2011.
- [7] C. Walker and I. Anderson, "From land to water: bringing dielectric elastomer sensing to the underwater realm," in *Electroactive Polymer Actuators and Devices (EAPAD) 2016*, vol. 9798. SPIE, Conference Proceedings, pp. 443–450.
- [8] C. Jean-Mistral, G. Jacquet-Richardet, and A. Sylvestre, "Parameters influencing fatigue life prediction of dielectric elastomer generators," *Polymer Testing*, vol. 81, no. 8, 2020.
- [9] F. B. Madsen, A. E. Daugaard, S. Hvilsted, and A. L. Skov,
  - "The current state of silicone-based dielectric elastomer transducers," *Macromolecular Rapid Communications*, vol. 37, no. 5, pp. 378–413, 2016. [Online]. Available: https://onlinelibrary.wiley.com/doi/abs/10. 1002/marc.201500576
- [10] P. Brochu and Q. Pei, "Advances in dielectric elastomers for actuators and artificial muscles," *Macromolecular Rapid Communications*, vol. 31, no. 1, pp. 10–36, 2010. [Online]. Available: https: //onlinelibrary.wiley.com/doi/abs/10.1002/marc.200900425
- [11] G. Moretti, S. Rosset, R. Vertechy, I. Anderson, and M. Fontana, "A review of dielectric elastomer generator systems," *Advanced Intelligent* Systems, vol. 2, no. 10, 2020.
- [12] W. L. Robb, "Thin silicone membranes-their permeation properties and some applications," *Annals of the New York Academy of Sciences*, vol. 146, no. 1, pp. 119–137, 1968. [Online]. Available: https://nyaspubs. onlinelibrary.wiley.com/doi/abs/10.1111/j.1749-6632.1968.tb20277.x
- [13] P. Bian, Y. Wang, and T. J. McCarthy, "Rediscovering silicones: The anomalous water permeability of "hydrophobic" pdms suggests nanostructure and applications in water purification and anti-icing,"

- Macromolecular Rapid Communications, vol. 42, no. 5, p. 2000682, 2021. [Online]. Available: https://onlinelibrary.wiley.com/doi/abs/10. 1002/marc.202000682
- [14] F. B. Albuquerque and H. Shea, "Influence of humidity, temperature and prestretch on the dielectric breakdown strength of silicone elastomer membranes for deas," Smart Materials and Structures, vol. 29, no. 10, p. 105024, 2020. [Online]. Available: https: //dx.doi.org/10.1088/1361-665X/aba5e3
- [15] B. Fasolt, F. Welsch, M. Jank, and S. Seelecke, "Effect of actuation parameters and environment on the breakdown voltage of silicone dielectric elastomer films," Smart Materials and Structures, vol. 28, no. 9, p. 094002, 2019. [Online]. Available: https: //dx.doi.org/10.1088/1361-665X/ab2f34
- [16] B. Fasolt, F. B. Albuquerque, J. Hubertus, G. Schultes, H. Shea, and S. Seelecke, "Electrode impact on the electrical breakdown of dielectric elastomer thin films," *Polymers*, vol. 15, no. 20, 2023. [Online]. Available: https://www.mdpi.com/2073-4360/15/20/4071
- [17] E. Taine, A. Claverie, F. Caille, S. Seima, N. Fourdilis, J.-M. Hendrikse, and R. Boulard, "The S3 wave energy converter story," in *Electroactive Polymer Actuators, Sensors, and Devices (EAPAD) 2025*, S. S. Seelecke, A. L. Skov, K. Takagi, and J. D. W. Madden, Eds., vol. 13431, International Society for Optics and Photonics. SPIE, 2025, p. 134310I. [Online]. Available: https://doi.org/10.1117/12.3062263
- [18] K. Zakowski, M. Narozny, and M. Szocinski, "Influence of water salinity on corrosion risk - the case of the southern baltic sea coast," *Environmental monitoring and assessment*, vol. 186, 2014.
- [19] J. Crank, The Mathematics of Diffusion, second edition ed. Oxford University Press, 1975.
- [20] M. D. Placette, X. Fan, J.-H. Zhao, and D. Edwards, "Dual stage modeling of moisture absorption and desorption in epoxy mold compounds," *Microelectronics Reliability*, vol. 52, no. 7, pp. 1401– 1408, 2012. [Online]. Available: https://www.sciencedirect.com/science/ article/pii/S0026271412000820
- [21] D. Marx, "Proton transfer 200 years after von grotthuss: Insights from ab initio simulations," *ChemPhysChem*, vol. 7, no. 9, pp. 1848–1870, 2006. [Online]. Available: https://chemistry-europe.onlinelibrary.wiley.com/doi/abs/10.1002/cphc.200600128
- [22] E. Taine, T. Andritsch, I. A. Saeedi, and P. H. F. Morshuis, "Size effect and electrical ageing of pdms dielectric elastomer with competing failure modes," Smart Materials and Structures, vol. 32, no. 10, p. 105021, 2023. [Online]. Available: https://dx.doi.org/10.1088/1361-665X/acf53a
- [23] E. Taine, T. Andritsch, I. Saeedi, and P. Morshuis, "Dielectric breakdown strength of PDMS elastomers after mechanical cycling," *Energies*, vol. 16, no. 21, 2023. [Online]. Available: https://www.mdpi. com/1996-1073/16/21/7424
- [24] C. Zhang, Z. Lv, Z. Xu, K. Wu, P. Morshuis, and A. Claverie, "Influence of moisture absorption on space charge accumulation in liquid silicone rubber under high dc electric field," in *IEEE 5th International Conference on Dielectrics (ICD)*, Conference Proceedings, pp. 1–4.